

coils, thereby maintaining consistently high transfer efficiency. High-order PT-symmetric systems naturally support purely real eigenfrequencies that remain stable despite changes in transmission distance, allowing efficient energy transfer across a wide range. Together, these strategies help keep the system operating within the regime of purely real eigenvalues, ensuring robust and stable WPT. While these methods improve transmission efficiency and system robustness, they remain ineffective in complex energy transfer scenarios, such as robotic arms and electric insulator string configurations, where longer transmission distances and greater structural

deformations are required [20]. To further extend the transmission range, researchers have introduced relay coils to form a Domino chain, effectively overcoming the size constraints of individual coils [21–23]. However, this approach is highly sensitive to positional disturbances, as variations in coupling strength between coils lead to significant efficiency degradation. Furthermore, the cumulative parasitic resistance introduced by additional coils becomes increasingly non-negligible, further compromising overall transmission efficiency. These inherent limitations fundamentally restrict the practical deployment of Domino chain-based systems in complex

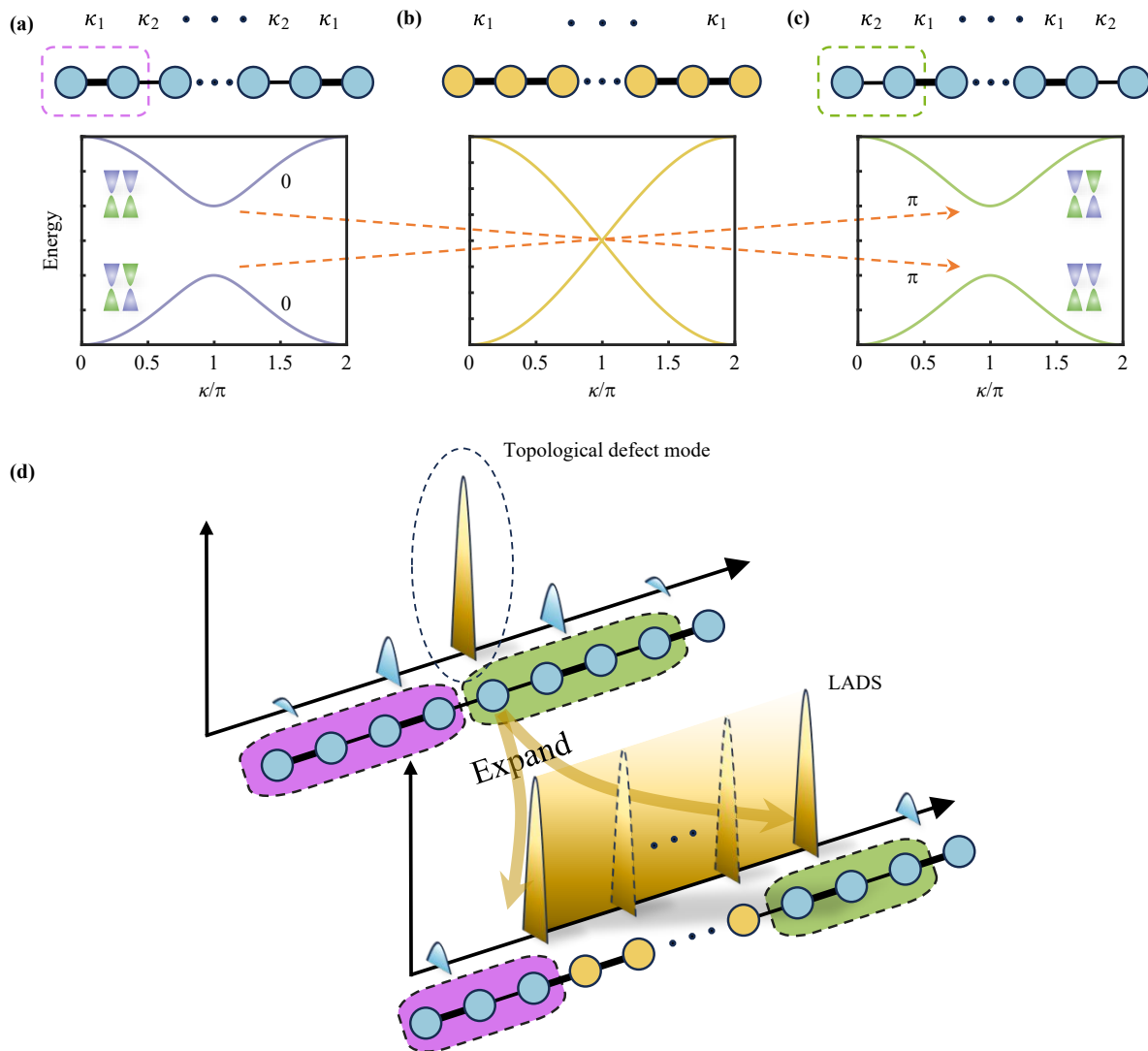


Fig. 1 Schematic of the topological LADS and enhanced homogeneous field. (a–c) Topological phase transition of the dimer chain. The dashed box represents the unit cell containing two sites, where the intra-cell and inter-cell coupling strength are κ_1 and κ_2 , respectively. The thick (thin) line between two sublattices represents strong (weak) coupling strength with $\kappa_1 > \kappa_2$. A topological transition occurs in (b) with the uniform coupling strength κ_1 between adjacent site. The band gap reopens as the coupling strength changes. (d) Schematics of LADS expanded from the topological defect state in the heterojunction dimer chain. The topological defect state appears at the interface between two topological distinguished chains. After expanding the single interface site to a chain with uniform coupling strength, the edge state is expanded in a large area.

environments.

The integration of topological photonics with near-field WPT has recently enabled robust energy transmission through unique state distributions [24–29]. For instance, researchers have implemented Su–Schrieffer–Heeger (SSH) chains with coil resonators, which supports topologically protected edge states [30, 31]. These states exhibit strong immune against positional perturbations, ensuring stable energy delivery. However, because energy is predominantly localized at the terminal sites of the chain, this approach restricts power transfer to a single receiver [25–27], making it unsuitable for simultaneous multi-load WPT. Recent advances in topological photonics have sparked growing interest in large-area topological edge states associated with topological phase transition, which offer exceptional robustness against structural disorder while enabling spatially extended field confinement [32–35]. Unlike conventional localized edge modes, these states facilitate electromagnetic wave manipulation over extended geometries while preserving topological protection — an essential feature for applications in low-loss multi-channel energy transfer [36]. Experimental realizations in non-Hermitian photonic crystals [37–39], acoustics [40–42], and waveguide platforms [43, 44] have further demonstrated the feasibility of large-area topological transport. Given these advantages, incorporating the large area topological physics mechanism into WPT presents a promising avenue for enhancing efficiency and scalability.

In this work, we present a pioneering study on topological large-area defect states (LADSs) for multi-load WPT. By inserting a gapless chain of uniformly coupled resonators at the interface of two topologically distinct SSH configurations, we experimentally demonstrate the emergence of LADS with a uniform state distribution across multiple target sites. This unique energy localization enables simultaneous multi-load charging, which we conduct a visual experimental demonstration using Light Emitting Diode (LED) lamps as representative loads. Furthermore, we systematically investigate the robustness of LADS against external perturbations, highlighting its resilience to positional misalignment and structural disorder. The findings of this work provide valuable insights into the potential of topological physics in advancing WPT technologies, particularly for applications requiring spatially distributed energy delivery with enhanced stability.

2 Results

2.1 LADS in a composite topological chain

Figures 1(a)–(c) show the topological transition of SSH chain with three different configurations. κ_1 and κ_2 represent the coupling between adjacent atoms, where κ_1 denotes the strong coupling strength and κ_2 corresponds to the weak coupling strength. When the intracell coupling exceeds the intercell coupling, the system

resides in a topologically trivial phase characterized by a Zak phase of 0 [45]. Under open boundary conditions, the energy spectrum exhibits two distinct bands separated by a finite bandgap, with no edge states present, as shown in Fig. 1(a). Conversely, when the intracell coupling becomes weaker than the intercell coupling, the system transitions into a topologically nontrivial phase where the Zak phase equals π . This phase supports the emergence of topologically protected edge states localized at the boundaries. At the critical point where two coupling strengths are equal, the bandgap closes and subsequently reopens, signifying a topological phase transition. The Zak phases corresponding to the topologically trivial and nontrivial phases are indicated near the respective bands. In Fig. 1(d), a simple topological defect is introduced at the interface between two chains with distinct configurations, exhibiting weak coupling strengths to the edge atoms of both chains [46]. This heterojunction dimer chain realizes a defect state at zero energy. After expanding the interfacial atom into a uniformly coupled chain, the originally localized edge state is expanded to a LADS, with energy uniformly distributed across the odd sites.

Figure 2(a) depicts a chain consisting of 15 coil resonators. The parameters of each coil are maintained identical. The resonant frequency is 358 kHz, with a capacitance of 22 nF, and the diameter is standardized at 10 cm. The coupling strength between two resonators depends on their separation distance. Through experimental measurements, we extracted the relationship between the coupling strength and separation distance of coils, as shown in Fig. 2(b). The coupling strength between two coils corresponds to half the frequency splitting in the spectrum. The measured results and fitted curve are represented by red dots and solid line, respectively. The fitted function between coupling strength κ and distance d is $\kappa = 79e^{-d/2.29} + 6.08$ [47]. Guided by this quantitative correlation, precise control of coupling between adjacent coils can be effectively implemented. Then we employed a small loop antenna connected to a vector network analyzer (VNA) to detect the density of states (DOS) of the system based on the principle of near-field probing [48]. Owing to the substantial frequency detuning between the probe and the coil resonators' frequency, the loop antenna could be approximated as a high-impedance probing element. The antenna is positioned at the center of the test coil, so energy can be injected into the system through the antenna. By measuring the reflection coefficient S_{11} , the local density of states (LDOS) can be obtained using $1 - |S_{11}|^2$. The DOS of the topological chain is derived by summing and averaging the LDOS contributions of all coils.

We initially construct a heterojunction dimer chain comprising nine coil resonators to study the topological defect state [46]. Figure 3(a) shows the schematic of the composite dimer chain composed of two topological

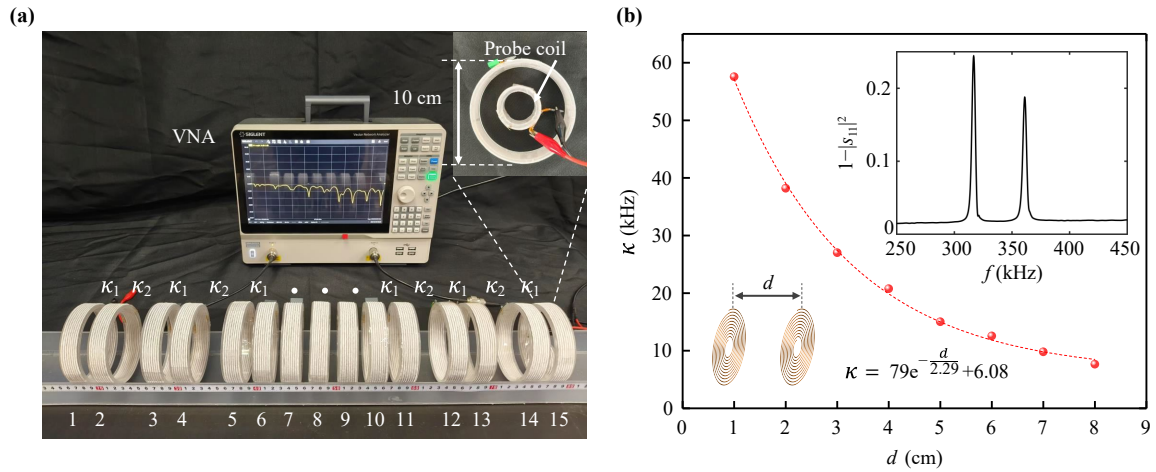


Fig. 2 Experimental setup and the coupling strength κ as a function of the distance d between two adjacent coils. (a) The topological chain composed of 15 coil resonators. The diameter and the resonant frequency of the coil are 10 cm and 358 kHz, respectively. The loaded capacitor is 22 nF. The inset shows the probe coil used for measuring the reflection spectrum. (b) The coupling strength at different distances and fitted curve. The red dots are the measured results and the dashed line is the fitted curve. The fitting function is $\kappa = 79e^{-d/2.29} + 6.08$. The inset shows the measured frequency spectrum when $d = 4$ cm.

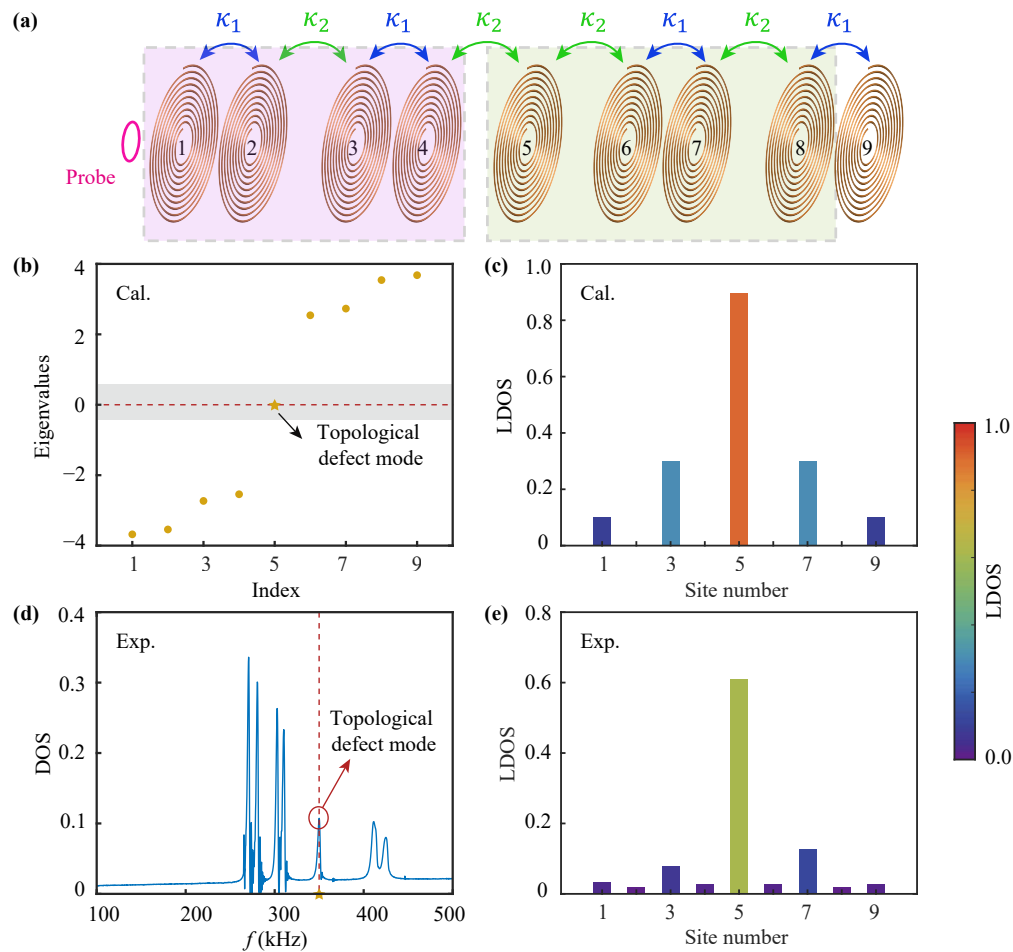


Fig. 3 Topological defect state in heterojunction dimer chain with $\kappa_1/\kappa_2 = 3$. (a) Schematic of the composite dimer chain composed of two topological distinguished chains. (b) The corresponding eigenvalues spectra of the heterojunction topological chain. The topological defect state is marked by the arrow. (c) Calculated LDOS distribution of topological defect state. (d) Measured DOS spectrum of the heterojunction topological chain. The topological defect state at 350 kHz is marked by the circle. (e) Measured LDOS distribution of topological defect state.

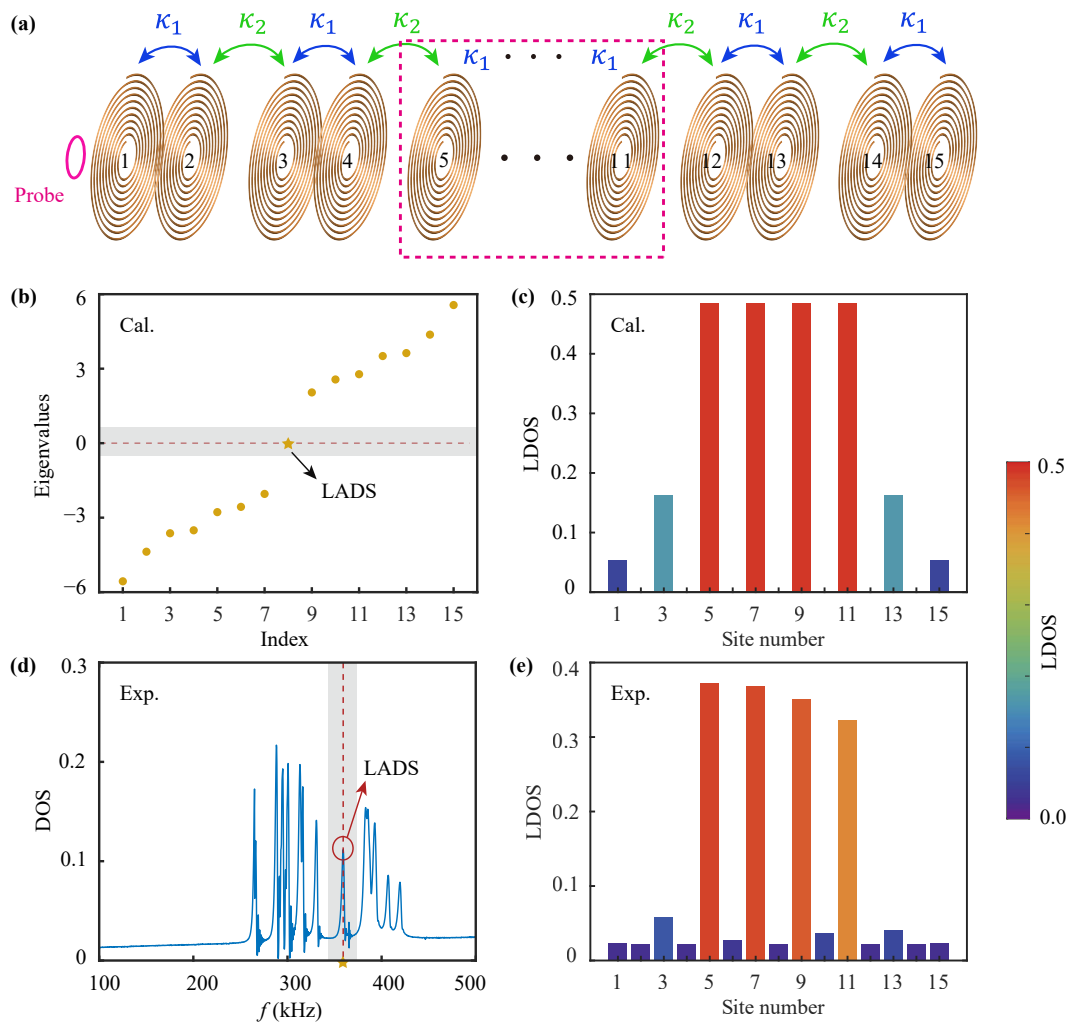


Fig. 4 Topological LADS in heterojunction dimer chain with $\kappa_1/\kappa_2 = 3$. (a) Schematic of the expanded dimer chain. (b) The real part of the energy spectrum. The zero mode corresponds to LADS. (c) Calculated LDOS distribution of LADS. (d) Measured DOS spectrum of the expanded dimer chain. The frequency of the LADS is 358 kHz because of the next-nearest-coupling and errors generated during coil sample preparation. One bulk state (260 kHz) is also marked by the circle. (e) Measured LDOS distribution of LADS.

distinguished chains. By calculating the eigenvalues of the system, we can find an isolated mode at the zero energy, which corresponds to the topological defect state, as shown in Fig. 3(b). The topological defect mode is marked by the arrow. From the calculated LDOS distribution of the topological defect state in Fig. 3(c), it can be found that the energy is mainly concentrated on the resonators at the interface. Moreover, the measured DOS spectrum and LDOS distributions are shown in Figs. 3(d) and (e), respectively. An isolated state at the bandgap can be easily determined from the DOS spectrum, and the measured LDOS results are meet well with the calculated ones.

We further expand the single coil at the interface site to seven uniformly coupled coils, where the coupling strength between each coil is κ_1 . The expanded dimer chain is schematically shown in Fig. 4(a). From the calculated eigenvalues in Fig. 4(b), we can see the

isolated LADS in the bandgap. Especially, the LADS is highly localized at multiple sites instead of one fixed site, as shown in Fig. 4(c). Like Fig. 3, we also measured DOS spectrum and LDOS distribution of the LADS, as shown in Figs. 4(d) and (e), respectively. The LADS (i.e., 360 kHz) exists in the bandgap and is circled by the red circle. At this time, the energy is uniformly distributed at the odd-positioned coils. The slight differences between experimental results and theoretical calculations stem from sample construction and testing errors.

Subsequently, we employ LED indicators to visualize the state distribution of LADS. The chain is excited by a high-power signal source (AG Series Amplifier, T&C Power Conversion), with a source coil positioned at the edge of the uniformly coupled coil resonators to establish LADS. Each resonant coil is added with an LED indicator through non-resonant coil. When the magnetic field

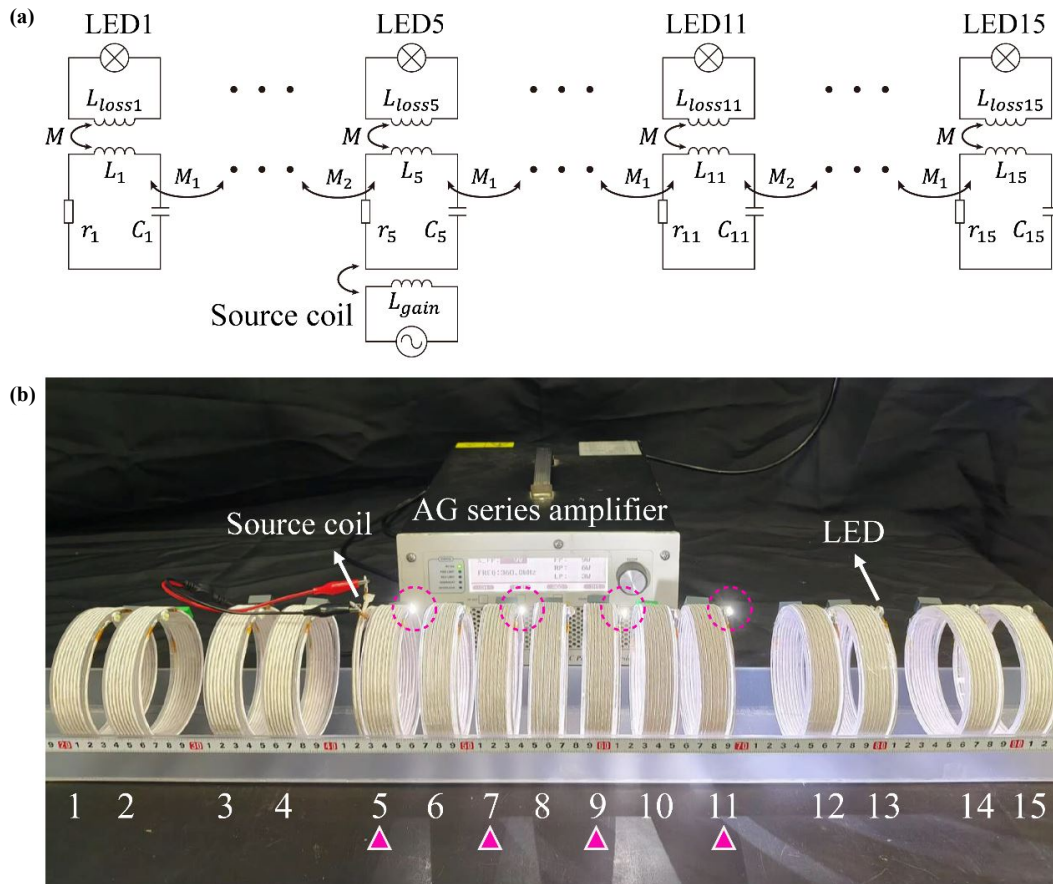


Fig. 5 Experimental demonstration of the 3 W WPT for lighting LED lamps. **(a)** The circuit diagrams of the system. **(b)** The source coil is placed at the edge of the uniformly coupled coils. The LED lamps are mounted on all the resonant coils. At the working frequency, the energy of the LADS is predominantly localized at sites 5, 7, 9, and 11, with corresponding LEDs at these sites being illuminated. In contrast, LEDs at other sites remain dark due to the relatively weak magnetic field.

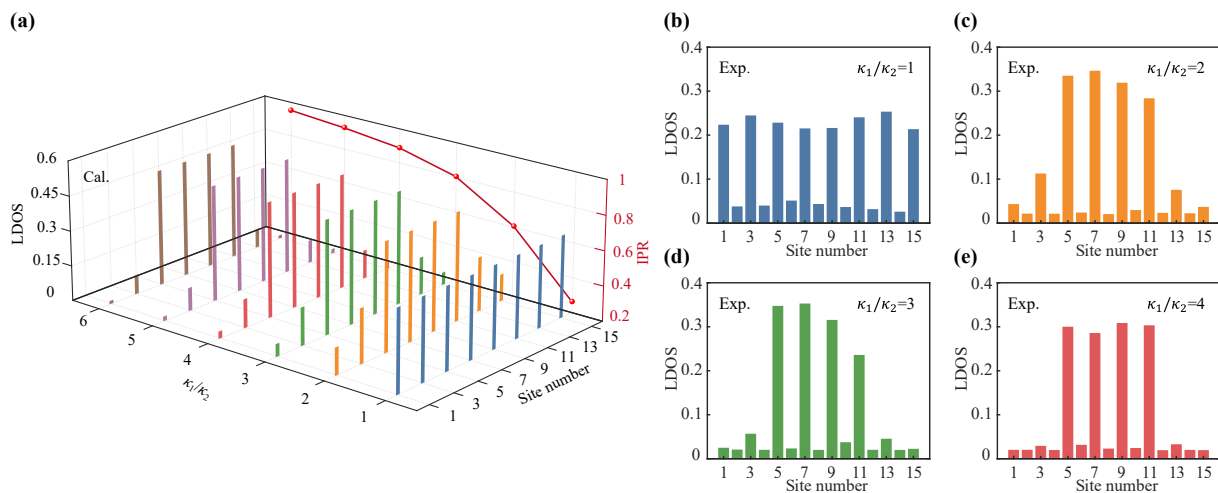


Fig. 6 LDOS and inverse participation ratio (IPR) with different coupling strength. **(a)** Calculated LDOS distributions and IPR. When $\kappa_1/\kappa_2=1$, the field strength on each unit is equal. As the increase of κ_1 , the energy is more localized on the expanded units. IPR rises from 0.25 to 0.95. **(b–e)** Measured LDOS distributions. Here we fix κ_2 at 15 kHz and the values of κ_1 are 15 kHz, 30 kHz, 45 kHz and 60 kHz, respectively.

strength on a resonant coil exceeds a critical threshold, working frequency of LADS, the LED indicators at the the corresponding LED indicator is illuminated. At the 5, 7, 9 and 11 sites are lit up, while all other indicators

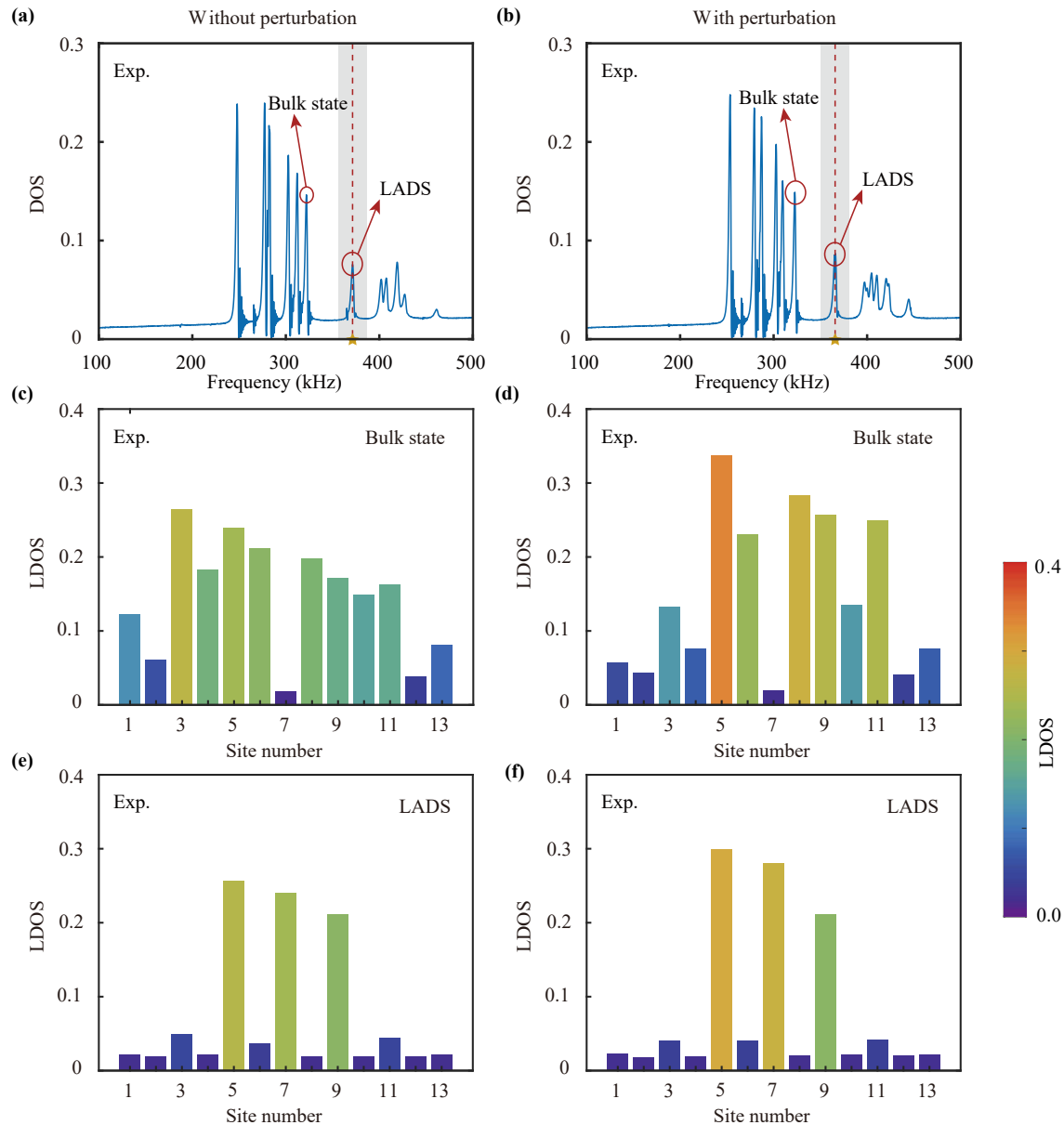


Fig. 7 Robust LADS in an expanded composite topological chain composed of 13 coils. **(a, b)** Measured DOS spectrum without (with) perturbation. **(c, d)** Measured LDOS distributions of the bulk state without (with) perturbation. **(e, f)** Measured LDOS distributions of the LADS without (with) perturbation.

remain dark, as illustrated in Fig. 5. As a result, the design of LADS for multi-load charging is intuitively demonstrated.

2.2 Characterization of LADS

The energy localization degree of LADS varies under different coupling conditions. We calculate LDOS of the system for κ_1/κ_2 ranging from 1 to 6, as shown in Fig. 6(a). The inverse participation ratio (IPR) is defined as $\sum_n |\phi_n|^4 / (\sum_n |\phi_n|^2)^2$, which serves as a standard metric for quantifying localization [49, 50]. The IPR exhibits a pronounced increasing trend with the

progressive enhancement of κ_1 . In the experimental configuration, with κ_2 fixed at 15 kHz and κ_1 incrementally set to 15, 30, 45 and 60 kHz, the energy distribution demonstrates progressive concentration on the uniformly coupled coils as κ_1 increases, as shown in Figs. 6(b)–(e), respectively.

2.3 Robustness against perturbations

We experimentally investigated the robustness of LADS against positional perturbations. A topological chain comprising 13 coil resonators was constructed. Currently κ_1 is 15 kHz and κ_2 is 45 kHz, corresponds to 5.5 cm

and 1.5 cm, respectively. The perturbations are introduced by randomly varying the distance between adjacent coils. We first generate random numbers within the range of 0 to 1, then multiply by a displacement factor $\Delta d = 0.5$ cm to determine the change of the distance between adjacent coils. We select a bulk state for comparison. It can be observed that there was no significant change in the frequencies of both LADS and bulk state after the introduction of perturbations. The LDOS of bulk state and LADS are also measured. There is a significant change in the state distribution of the bulk state, whereas the energy of LADS remains concentrated on the central three coil resonators, only a slight variation in amplitude compared to the unperturbed case. These findings demonstrate that LADS exhibits strong robustness against positional perturbations.

3 Conclusion

In summary, we have experimentally demonstrated a novel approach to achieving LADS in a one-dimensional topological WPT system based on subwavelength coil resonators. By leveraging the topological properties of SSH chains, we established a robust defect state that enables efficient and simultaneous power delivery to multiple spatially distributed loads. Unlike conventional topological WPT schemes, where energy localization is confined to the system's edges, our approach extends the energy distribution over a broader region while maintaining resilience against positional perturbations and structural disorder. This work provides a foundational framework for multi-load WPT, paving the way for practical implementations in scenarios demanding spatial flexibility and enhanced stability. The demonstrated topological mechanism is not only applicable to planar coil arrays but also holds the potential for higher-dimensional extensions, enabling new possibilities for robust and scalable wireless energy networks.

Declarations The authors declare no competing financial and non-financial interests.

Data availability All the data that support the findings of this study are available from the corresponding authors upon reasonable request.

Code availability All the codes that support the findings of this study are available from the corresponding authors upon reasonable request.

Author contributions Z. G. and H. C. conceived the idea and supervised the project. L. W. and H. Z. carried out the analytical calculations with the help of Y. L., Y. Y. and L. W. prepared the sample and conducted experimental measurements. L. W., H. Z. and Z. G. wrote the manuscript. All authors contributed to discussion of the results and the manuscript.

Acknowledgements This work was supported by the National Key R&D Program of China (Nos. 2021YFA1400602 and 2023YFA1407600), the National Natural Science Foundation of China (Nos. 12374294 and 52477014), and the Chenguang Program of Shanghai (No. 21CGA22).

References

1. M. Song, P. Jayathurathnage, E. Zanganeh, M. Krasikova, P. Smirnov, P. Belov, P. Kapitanova, C. Simovski, S. Tretyakov, and A. Krasnok, Wireless power transfer based on novel physical concepts, *Nat. Electron.* 4(10), 707 (2021)
2. A. P. Sample, D. T. Meyer, and J. R. Smith, Analysis, experimental results, and range adaptation of magnetically coupled resonators for wireless power transfer, *IEEE Trans. Ind. Electron.* 58(2), 544 (2011)
3. L. Wang, Y. Wang, Z. Guo, H. Jiang, Y. Li, Y. Yang, and H. Chen, Research progress in magnetic resonance wireless power transfer based on higher-order non-Hermitian physics, *Acta Phys. Sin.* 73(20), 201101 (2024)
4. K. Sun, R. Fan, X. Zhang, Z. Zhang, Z. Shi, N. Wang, P. Xie, Z. Wang, G. Fan, H. Liu, C. Liu, T. Li, C. Yan, and Z. Guo, An overview of metamaterials and their achievements in wireless power transfer, *J. Mater. Chem. C* 6(12), 2925 (2018)
5. A. Christ, A. Fallahi, E. Neufeld, Q. Balzano, and N. Kuster, Mechanism of capacitive coupling of proximal electromagnetic sources with biological bodies, *Bioelectromagnetics* 43(7), 404 (2022)
6. C. Liu, A. P. Hu, and N. K. C. Nair, Modelling and analysis of a capacitively coupled contactless power transfer system, *IET Power Electron.* 4(7), 808 (2011)
7. M. P. Theodoridis, Effective capacitive power transfer, *IEEE Trans. Power Electron.* 27(12), 4906 (2012)
8. F. Lu, H. Zhang, and C. Mi, A review on the recent development of capacitive wireless power transfer technology, *Energies* 10(11), 1752 (2017)
9. Y. Zhang, S. Chen, X. Li, and Y. Tang, Design of high-power static wireless power transfer via magnetic induction: An overview, *CPSS Trans. Power Electron. Appl.* 6(4), 281 (2021)
10. A. Kurs, A. Karalis, R. Moffatt, J. D. Joannopoulos, P. Fisher, and M. Soljacic, Wireless power transfer via strongly coupled magnetic resonances, *Science* 317(5834), 83 (2007)
11. H. Li, J. Li, K. Wang, W. Chen, and X. Yang, A maximum efficiency point tracking control scheme for wireless power transfer systems using magnetic resonant coupling, *IEEE Trans. Power Electron.* 30(7), 3998 (2015)
12. S. Assaworarith, X. Yu, and S. Fan, Robust wireless power transfer using a nonlinear parity-time-symmetric circuit, *Nature* 546(7658), 387 (2017)
13. J. L. Zhou, B. Zhang, W. X. Xiao, D. Y. Qiu, and Y. F. Chen, Nonlinear parity-time-symmetric model for constant efficiency wireless power transfer: Application to a drone-in-flight wireless charging platform, *IEEE Trans. Ind. Electron.* 66(5), 4097 (2019)

14. S. Assaworrorarit and S. Fan, Robust and efficient wireless power transfer using a switch-mode implementation of a nonlinear parity–time symmetric circuit, *Nat. Electron.* 3(5), 273 (2020)
15. X. Hao, K. Yin, J. Zou, R. Wang, Y. Huang, X. Ma, and T. Dong, Frequency-stable robust wireless power transfer based on high-order pseudo-Hermitian physics, *Phys. Rev. Lett.* 130(7), 077202 (2023)
16. M. Sakhdari, M. Hajizadegan, and P. Y. Chen, Robust extended-range wireless power transfer using a higher-order PT-symmetric platform, *Phys. Rev. Res.* 2(1), 013152 (2020)
17. Y. Qu, B. Zhang, W. Gu, and X. Shu, Wireless power transfer system with high-order compensation network based on parity-time-symmetric principle and relay coil, *IEEE Trans. Power Electron.* 38(1), 1314 (2023)
18. Z. Guo, J. Jiang, X. Wu, H. Zhang, S. Hu, Y. Wang, Y. Li, Y. Yang, and H. Chen, Rotation manipulation of high-order PT-symmetry for robust wireless power transfer, *Fundam. Res.*, doi: 10.1016/j.fmre.2023.11.010 (2023)
19. Z. Guo, F. Yang, H. Zhang, X. Wu, Q. Wu, K. Zhu, J. Jiang, H. Jiang, Y. Yang, Y. Li, and H. Chen, Level pinning of anti-PT symmetric circuits for efficient wireless power transfer, *Natl. Sci. Rev.* 11(1), nwad172 (2023)
20. C. Zhang, D. Lin, N. Tang, and S. Y. R. Hui, A novel electric insulation string structure with high-voltage insulation and wireless power transfer capabilities, *IEEE Trans. Power Electron.* 33(1), 87 (2018)
21. C. K. Lee, W. X. Zhong, and S. Y. R. Hui, Effects of magnetic coupling of nonadjacent resonators on wireless power Domino-resonator systems, *IEEE Trans. Power Electron.* 27(4), 1905 (2012)
22. D. Ahn and S. Hong, A study on magnetic field repeater in wireless power transfer, *IEEE Trans. Ind. Electron.* 60(1), 360 (2013)
23. W. X. Zhong, C. K. Lee, and S. Y. R. Hui, General analysis on the use of Tesla’s resonators in Domino forms for wireless power transfer, *IEEE Trans. Ind. Electron.* 60(1), 261 (2013)
24. J. Feis, C. J. Stevens, and E. Shamoniina, Wireless power transfer through asymmetric topological edge states in diatomic chains of coupled meta-atoms, *Appl. Phys. Lett.* 117(13), 134106 (2020)
25. F. Yang, J. Song, Z. Guo, X. Wu, K. Zhu, J. Jiang, Y. Sun, Y. Jiang, and H. Chen, Actively controlled asymmetric edge states for directional wireless power transfer, *Opt. Express* 29(5), 7844 (2021)
26. J. Song, F. Yang, Z. Guo, X. Wu, K. Zhu, J. Jiang, Y. Sun, Y. Li, H. Jiang, and H. Chen, Wireless power transfer via topological modes in dimer chains, *Phys. Rev. Appl.* 15(1), 014009 (2021)
27. L. Zhang, Y. Yang, Z. Jiang, Q. Chen, Q. Yan, Z. Wu, B. Zhang, J. Huangfu, and H. Chen, Demonstration of topological wireless power transfer, *Sci. Bull. (Beijing)* 66(10), 974 (2021)
28. K. Yatsugi, S. E. Pandarakone, and H. Iizuka, Higher-order topological corner state in a reconfigurable breathing Kagome lattice consisting of magnetically coupled LC resonators, *Sci. Rep.* 13(1), 8301 (2023)
29. J. Jiang, S. Hu, Z. Guo, S. Ke, X. Wu, Y. Wu, Y. Wang, H. Jiang, Y. Yang, and H. Chen, Topological corner states for wireless power transfer, *Rev. Phys.* 13, 100112 (2025)
30. H. Zhang, H. Li, J. Jiang, H. Jiang, Y. Sun, Y. Yang, H. Chen, and Z. Guo, Observation of robust polarization conversion via topological edge states in dimer chains, *J. Opt.* 27(4), 045401 (2025)
31. Z. Guo, J. Jiang, X. Wu, S. L. Ke, X. Q. Su, H. Jiang, Y. Sun, Y. Li, J. Ren, Y. Yang, Z. Yu, and H. Chen, 1D photonic topological insulators composed of split ring resonators: A mini review, *Adv. Physiol. Res.* 6, 2300125 (2024)
32. L. Du, Y. Liu, M. Li, X. Zhou, S. Wang, Q. Zhao, Z. Li, L. Tao, X. Xiao, K. Song, and X. Zhao, Dual-band large-area topological edge states and higher-order corner states in a valley Hall photonic crystal, *Phys. Rev. B* 110(15), 155415 (2024)
33. Z. Li, S. Li, B. Yan, H. Chan, J. Li, J. Guan, W. Bi, Y. Xiang, Z. Gao, S. Zhang, P. Zhan, Z. Wang, and B. Xie, Symmetry-related large-area corner mode with a tunable mode area and stable frequency, *Phys. Rev. Lett.* 134(11), 116607 (2025)
34. M. Wang, R. Y. Zhang, L. Zhang, D. Wang, Q. Guo, Z. Q. Zhang, and C. T. Chan, Topological one-way large-area waveguide states in magnetic photonic crystals, *Phys. Rev. Lett.* 126(6), 067401 (2021)
35. S. Yan, J. Yang, S. Shi, Z. Zuo, C. Wang, and X. Xu, Transport of a topologically protected photonic waveguide on-chip, *Photon. Res.* 11(6), 1021 (2023)
36. L. He, Z. Lan, B. Yang, J. Yao, Q. Ren, J. W. You, W. E. Sha, Y. Yang, and L. Wu, Experimental observation of topological large-area pseudo-spin-momentum-locking waveguide states with exceptional robustness, *Adv. Photon. Nexus* 3(1), 016009 (2024)
37. Z. Lan, M. L. N. Chen, J. W. You, and W. E. Sha, Large-area quantum-spin-Hall waveguide states in a three-layer topological photonic crystal heterostructure, *Phys. Rev. A* 107(4), L041501 (2023)
38. Z. Hu, M. Qin, L. He, W. Liu, T. Yu, S. Xiao, and Q. Liao, Manipulating the optical beam width in topological pseudospin-dependent waveguides using all-dielectric photonic crystals, *Opt. Lett.* 47(20), 5377 (2022)
39. X. Yu, J. Chen, Z. Y. Li, and W. Liang, Topological large-area one-way transmission in pseudospin-field-dependent waveguides using magneto-optical photonic crystals, *Photon. Res.* 11(6), 1105 (2023)
40. J. Q. Wang, Z. D. Zhang, S. Y. Yu, H. Ge, K. F. Liu, T. Wu, X. C. Sun, L. Liu, H. Y. Chen, C. He, M. H. Lu, and Y. F. Chen, Extended topological valley-locked surface acoustic waves, *Nat. Commun.* 13(1), 1324 (2022)
41. S. Yin, L. Ye, H. He, M. Ke, and Z. Liu, Acoustic valley-locked waveguides in heterostructures of a square lattice, *Phys. Rev. Appl.* 18(5), 054073 (2022)
42. M. Wang, W. Zhou, L. Bi, C. Qiu, M. Ke, and Z. Liu, Valley-locked waveguide transport in acoustic heterostructures, *Nat. Commun.* 11(1), 3000 (2020)
43. T. Qu, N. Wang, M. Wang, L. Zhang, and J. Chen, Flexible electromagnetic manipulation by topological one-way large-area waveguide states, *Phys. Rev. B* 105(19), 195432 (2022)

44. Q. Chen, L. Zhang, F. Chen, Q. Yan, R. Xi, H. Chen, and Y. Yang, Photonic topological valley-locked waveguides, *ACS Photonics* 8(5), 1400 (2021)
45. P. Delplace, D. Ullmo, and G. Montambaux, Zak phase and the existence of edge states in graphene, *Phys. Rev. B* 84(19), 195452 (2011)
46. A. Blanco-Redondo, I. Andonegui, M. J. Collins, G. Harari, Y. Lumer, M. C. Rechtsman, B. J. Eggleton, and M. Segev, Topological optical waveguiding in silicon and the transition between topological and trivial defect states, *Phys. Rev. Lett.* 116(16), 163901 (2016)
47. Z. Guo, H. Jiang, Y. Li, H. Chen, and G. S. Agarwal, Enhancement of electromagnetically induced transparency in metamaterials using long range coupling mediated by a hyperbolic material, *Opt. Express* 26(2), 627 (2018)
48. J. Jiang, Z. Guo, Y. Ding, Y. Sun, Y. Li, H. Jiang, and H. Chen, Experimental demonstration of the robust edge states in a split-ring-resonator chain, *Opt. Express* 26(10), 12891 (2018)
49. B. Zhu, Q. Wang, D. Leykam, H. Xue, Q. Wang, and Y. D. Chong, Anomalous single-mode lasing induced by nonlinearity and the non-Hermitian skin effect, *Phys. Rev. Lett.* 129(1), 013903 (2022)
50. H. Qin, Z. Zhang, Q. Chen, and R. Fleury, Disclination states in nonreciprocal topological networks, *Phys. Rev. Res.* 6(1), 013031 (2024)